## 74110\_Auto\_Edited-check.docx

Radiomics and nomogram of magnetic resonance imaging for preoperative prediction of microvascular invasion in small hepatocellular carcinoma

Chen YD et al. MRI evaluating MVI of small-HCC

Yi-Di Chen, Ling Zhang, Zhi-Peng Zhou, Bin Lin, Zi-Jian Jiang, Cheng Tang, Yi-Wu Dang, Yu-Wei Xia, Bin Song, Li-Ling Long

#### Abstract

#### **BACKGROUND**

The microvascular invasion (MVI) of small hepatocellular carcinoma (sHCC) (≤ 3.0 cm) is an independent prognostic factor for poor progression free survival and overall survival. Radiomics can help extract imaging information associated with tumor pathophysiology.

#### AIM

To develop and validate radiomics scores and nomogram of gadolinium ethoxybenzyl dimeglumine (Gd-EOB-DTPA)-enhanced magnetic resonance imaging (MRI) for preoperative prediction of MVI in sHCC.

#### **METHODS**

Two hundred and twenty-one retrospective patients, external ninety-four and one hundred prospective patients were included in this multi-center study, all of the 415 patients were diagnosed as sHCC by postoperative pathology. Radiomics models of Gd-EOB-DTPA enhanced MRI and diffusion weighted imaging (DWI) were constructed and validated by machine learning. As presented in the radiomics nomogram, a prediction model was developed using multivariable logistic regression analysis which included the radiomics scores, radiologic features, and clinical features such as alpha-fetoprotein (AFP) level. The calibration, decision-making curve and clinical usefulness of radiomics nomogram were analyzed. The radiomics nomogram was validated by

external independent cohort data. The values of areas under the receiver operating curve (AUC) were used to assess the predictive capability.

#### **RESULTS**

Pathological examination confirmed MVI in 64 (28.9%), 22 (23.4%) and 16 (16.0%) of 221, 94, and 100 patients. AFP, tumor size, nonsmooth tumor margin, incomplete capsule, and peritumoral hypointensity in the hepatobiliary phases (HBP) images had poor diagnostic value for MVI of sHCC. Quantitative radiomics features (1409) of MRI were extracted. The classifier of logistic regression (LR) was the best machine learning method, the radiomics scores of HBP and DWI had the great diagnostic efficiency for prediction of MVI, in the testing set (hospital A) and validation set (hospital B, C) the AUC of HBP was 0.979, 0.970, and 0.803, the AUC of DWI was 0.971, 0.816, and 0.801 (*P* < 0.05). The good calibration and discrimination of radiomics and clinic combine nomogram model were exhibited in the testing and two external validation cohorts (C-index of HBP and DWI was 0.971, 0.912, 0.808 and 0.970, 0.843, 0.869, respectively). The clinical usefulness of the nomogram had been further confirmed by decision curve analysis.

#### CONCLUSION

AFP and conventional Gd-EOB-DTPA enhanced MRI features have poor diagnostic accuracy for MVI in sHCC patients. Machine learning with LR classifier has the best radiomics score in HBP and DWI. The developed radiomics nomogram as a noninvasive preoperative prediction method shows favorable predictive accuracy for evaluate MVI in sHCC.

**Key Words:** Magnetic resonance imaging; Hepatocellular carcinoma; Radiomics; Nomogram

Chen YD, Zhang L, Zhou ZP, Lin B, Jiang ZJ, Tang C, Dang YW, Xia YW, Song B, Long LL. Radiomics and nomogram of magnetic resonance imaging for preoperative prediction of microvascular invasion in small hepatocellular carcinoma. *World J Gastroenterol* 2022; In press

Core Tip: Microvascular invasion (MVI) accounts for about 20% of the small hepatocellular carcinoma (sHCC) (≤ 3.0 cm), it is a poor independent prognostic factor for progression-free survival and overall survival. However, there is no literature for report how to preoperatively predict MVI of sHCC. This multi-center study was developed and validated radiomics scores and nomogram of gadoxetic acid-enhanced magnetic resonance imaging (MRI) for predicting of MVI in sHCC preoperatively, the results demonstrated AFP and conventional gadolinium ethoxybenzyl dimeglumine enhanced MRI features have poor diagnostic accuracy for MVI in patients with sHCC, the radiomics scores of HBP and diffusion weighted imaging can improve the ability to predict MVI, and as a noninvasive preoperative prediction method, the radiomics nomogram of this study shows a favorable predictive accuracy in evaluating MVI of sHCC, which may help reassess the clinical therapeutic regimen of patients with sHCC.

#### 21 INTRODUCTION

Hepatocellular carcinoma (HCC) is the fourth most common cause of cancer-related death and ranks 6<sup>th</sup> in terms of incident cases worldwide<sup>[1]</sup>. HCC is an important public health problem in the world and the rate of death has increased for the past few years<sup>[2,3]</sup>. The size cutoff to define small HCC (sHCC) has been adopted to be 3.0 cm<sup>[4]</sup>. Although the prognosis of sHCC is better than that of other types of HCC, the higher postoperative recurrence result in the long-term outcome after resection of sHCC is far from satisfactory<sup>[5]</sup>. Previous studies have confirmed that the tumor size, higher tumor stage, worse histological differentiation and presence of microvascular invasion (MVI) are significant risk factors for short-term recurrence of HCC<sup>[6-8]</sup>. Particularly the incidence of MVI, which is an independent poorer prognostic factor for progression-free

survival and overall survival of sHCC patients, is generally about 20% in sHCC<sup>[9]</sup>. The presence or absence of MVI also suggests different therapeutic options for HCC. Research indicated that transcatheter arterial chemoembolization plus intensity-modulated radiotherapy combined with sorafenib showed obvious clinical benefit in HCC patients with MVI<sup>[10]</sup>. For sHCC with MVI, enlarged hepatectomy may be necessary.

The pathological examination of postoperative specimens is a gold standard for the presence of MVI<sup>[11]</sup>. However, postoperative specimens have the hysteresis, which is not ideal to guide the decision making of treatment. Besides being an invasive method, biopsy carries some risks of bleeding or tumor seeding<sup>[12]</sup>. Gadolinium ethoxybenzyl dimeglumine (Gd-EOB-DTPA) contrast enhanced liver magnetic resonance imaging (MRI) is a noninvasive test used to diagnosis a variety of liver diseases<sup>[13]</sup>, it could be useful to assess liver function in patients with various stages of liver disease<sup>[14]</sup>. Gd-EOB-DTPA MRI have been used to predict MVI based on tumor size, nonsmooth tumor margin, incomplete capsule and peritumor hypointensity in hepatobiliary phase<sup>[15-18]</sup>. But sHCC has a small size, regular margin, complete capsule (or no capsule) and usually free of peritumor hypointensity. Therefore, the traditional GD-EOB-DTPA MRI features are difficult to predict the MVI of sHCC.

As an emerging field, radiomics attempts to quantify tumor heterogeneity related to tumor parenchyma and microenvironment, including cellularity, extracellular matrix deposition, angiogenesis, necrosis and fibrosis<sup>[19,20]</sup>. Machine learning is a scientific method of algorithms and statistical models that using computer to interpret or predict patterns and inference<sup>[21]</sup>. In many medical situations, medical imaging can be analyzed by machine learning through a series of processes such as image registration, image segmentation, object detection, classification, and outcome prediction<sup>[22,23]</sup>. Automated computer algorithms can be used for quantitative image analysis, which can objectively quantify the heterogeneity of image by measuring the spatial variation of pixel intensity<sup>[24]</sup>. Radiomics with quantitative analysis provides a potential method for the diagnosis and prognosis of cancers<sup>[25,26]</sup>. Although few studies have explored the

feasibility of using radiomics based on computed tomography (CT) or MRI features to predict MVI in HCC<sup>[27-29]</sup>, but to our knowledge, previous studies did not involve the prediction of MVI in sHCC. Therefore, this research was aimed at exploring the further diagnostic value of liver Gd-EOB-DTPA MRI features in MVI of sHCC, and construct, validate the predictive efficacy of radiomics signatures and nomogram for MVI in sHCC. The study was also aimed to confirm the best modeling sequences, including images of T1 weighted imaging (T1WI), T2 weighted imaging (T2WI), diffusion weighted imaging (DWI), post-Gd-EOB-DTPA enhancement images of arterial phase (AP), portal vein phase (PVP), and hepatobiliary phase (HBP), for extracted radiomics signatures by machine learning.

## MATERIALS AND METHODS

#### Study cohort

The ethical institutional review board of our institution approved this multi-center and prospective validation study (No. 2019 KY-E-134). This study adhere the principles of Helsinki Declaration, and all prospective participants signed the informed consent. First step, we retrospectively searched our institution's (Guangxi Medical University First Affiliated Hospital, Hospital A) departmental electronic database for patients with consecutive hospital stays who had undergone upper-abdomen MRI between January 2016 and June 2020, a total of 221 patients were enrolled, who followed the inclusion criteria: (1) Patients received Gd-EOB-DTPA enhanced upper-abdomen MRI and "small HCC" (tumor size ≤ 3.0 cm) were diagnosed; (2) no macrovascular tumor invasion on MRI (i.e, no tumor thrombus in the hepatic or portal veins); (3) primary HCC were diagnosed by histopathologic examination within 2 wk after the MRI examination; and (4) MR images had sufficient image quality. Exclusion criteria of this study followed: (1) Patients who had undergone previous hepatobiliary surgery or liver directed therapy (i.e., transarterial chemoembolization or ablation); and (2) the lesions were diagnosed other than primary HCC. Second step, we prospectively recruited 94 and 100 participants as the independent validation sets from another two hospitals (Affiliated

Hospital of Guilin Medical University, and West China Hospital, Hospital B and C), between July 2021 and August 2021, who followed the same inclusion and exclusion. All patients underwent hepatectomy and pathologic assessment within 2 wk after the MRI examination. The alpha fetal protein (AFP), Child-Pugh grades (grade A to C) and the model for end-stage liver disease (MELD) scores were also analyzed and calculated for all patients (Figure 1).

#### Histopathologic analysis

Two experienced pathologists performed all histologic analyses in our central pathology lab. Edmondson-Steiner classification was used for identified the major histological grade of HCC. When a tumor within a vascular space lined by the endothelium, the MVI was confirmed that was visible only microscopically, documented the sites of positive MVI. All disagreements were resolved by consensus.

#### MRI examination

All patients underwent 3.0 T MRI with the sequences of Gd-EOB-DTPA enhancement and DWI (Discovery MR750, GE Healthcare, Waukesha, WI, United States; Prisma and MAGNETOM Verio, Siemens Healthcare, Erlangen, Germany), six sequences which including T1WI, T2WI, DWI and post-injection phases of EOB as AP, PVP, and HBP. Detailed descriptions of imaging acquisition protocols are summarized in Supplement Table 1. For advance DWI image quality, the respiratory triggering, Propeller and Resolve technical proposals were adopted.

#### Conventional radiological features analysis

Reporting and Data System (LI-RADS v2018) which included tumor size, AP hyperenhancement, blood products in mass, capsule, corona enhancement, delayed central enhancement, diffusion restriction, fat or iron in mass more than adjacent liver, fat or iron sparing in solid mass, mosaic appearance, hepatobiliary phase hypointensity,

hepatobiliary phase isointensity, and nodule-in-nodule appearance. The following MRI features were selected in this study: (1) Tumor size, the maximum diameter was measured on HBP axial images; (2) non-smooth tumor margin that was defined as nodular with extranodular growth or multinodular confluent; (3) incomplete capsule the region where the tumor border with liver tissue has no or incomplete capsule on portal venous phase or delayed phase; and (4) peritumoral hypointensity on HBP, wedge-shaped hypointense located outside of the tumor margin on HBP. After independently evaluated by three senior radiologists, discussions took place to reach consensus wherever discrepancies occurred.

## RADIOMICS SIGNATURES AND REPRODUCIBILITY ANALYSIS

Segmentation of the volume of interests

Transferred DICOM images into the big data intelligent analysis cloud platform (Huiying Medical Technology Co., Ltd., Beijing, China). Two experts on liver MRI (senior radiologists with 15 and 25 years of experience) reviewed all images respectively, and a radiologist manually segmented all target lesions who was blinded to the clinical information, creating a segmented volume of interest (VOI). After completion of VOIs by the more junior radiologist, the VOIs were reviewed by a senior radiologist for validation. To minimize the intensity variations caused by different scanning equipment and scanning parameters, these MR images were normalized by standard deviation ( $\mu$ -3 $\sigma$ ,  $\mu$  + 3 $\sigma$ ) before feature extraction, then automatically analyzed all delineated VOIs (Figure 2).

Since two radiologists measured the radiomics features, to assess the reproducibility, we calculated the intraclass correlation coefficient (ICC). When ICC > 0.80, the consistency was considered to be excellent.

#### Features extraction

We extracted 1409 quantitative imaging features from VOIs with the cloud platform big data intelligent analysis (http://radcloud.cn/). We categorized these features into four

groups. The first-order statistical features were taking as group 1 (including a total of 18 descriptors), which delineated the distribution of voxel intensities in the MR images through common and basic metrics. The group 2 included shape and size-based features (contained 14 three-dimensional features) that reflected the shape and size of the lesion areas. The group 3 included those features of two-order texture, grey level co-occurrence and grey level run-length texture matrices were used for calculated those features, 75 texture features been extracted for quantify heterogeneity of lesions. And the higher-order filter features as group 4, Laplacian, Wavelet, logarithmic and exponential filters were applied on medical images, and then the first-order statistics and texture features were extracted based on the filtered image (1302 filter features).

#### Features selection

The regression method of least absolute shrinkage and selection operator (LASSO) was used for decrease the irrelevance and redundancy. We performed the cross validation of 10-fold to select optimal feature subset in LASSO regression, which based on binomial deviance minimization criteria from the training cohort with the maximum iteration of 2000. The variance threshold of 0.8 that was used for selected eigenvalues of the variance.

#### Model development and validation

The retrospective data (Hospital A) were separated training dataset and testing dataset by random method with the ratio of 7:3, the prospective data (Hospital B and C) as the independent validation sets. After feature qualification, based on the selected features, several machine learning classifiers can be used for classification analysis, creating models that can separate or predict MVI-positive data. In this study, the radiomics-based Lasso models (machine learning) were constructed in T1WI, T2WI, DWI, AP, PVP and HBP, respectively. We selected K-nearest neighbor (KNN), support vector machin (SVM), extreme gradient boosting (XGBoost), random forest (RF), logistic regression

(LR) and decision tree (DT) as the ML classifiers, and the effectiveness of the model was improved by the validation method (Figure 2).

#### Confirmation of radiomics nomogram

R package (version 3.0, http://www.r-project.org/) was used for analysis of radiomics nomogram. Multivariable logistic regression analysis was performed to develop a model for predicting MVI, all variables associated with MVI at a significant level were candidates for stepwise multivariate analysis. Then constructed a nomogram which was formulated based on the results of multivariate logistic regression analysis. The receiver operating characteristic (ROC) curve was used for calculated the discrimination performance of established models, the values of area under the curve (AUC) were compared using the Delong non-parametric approach. The calibration of the radiomics model were assessed by calibration curves. The prospective data of independent validation sets (Hospital B and C) were used for tested the performance of the radiomics model. Finally, we conducted decision curves by calculating the net benefits for a range of threshold probabilities.

#### Statistical analyses

MedCalc 16.2.1 (Ostend, Belgium) and SPSS 22.0 (Armonk, NY, United States) were performed for statistical analyses. The method of Kolmogorov-Smirnov was performed for identify the normal distribution of continuous variables. Those differences of categorical variables and continuous variables were compered by  $\chi^2$  test or Fisher exact test, two-sample t-test or Mann-Whitney U test, respectively. ROC analyses were performed to evaluate the predictive performance for MVI of sHCC. Youden index was used for determining cut-off values, and then, area under the curve (AUC), sensitivity and specificity were calculated, Z test was used to compare those differences of AUCs. Statistical significance was considered when a two-sided P < 0.05.

#### RESULTS

#### Patients and serological examinations

A total of 415 qualified patients with sHCC were enrolled in the final study (Figure 1). In the hospital A, B, and C, the mean participant age was  $51.2 \pm 10.9$  (range 29-78) years,  $53.04 \pm 10.59$  (range 28-77) years, and  $54.01 \pm 10.82$  (range 28-85) years, respectively. Histological examination confirmed MVI was 64 (28.9%), 22 (23.4%), and 16 (16.0%), respectively. The number of patients with hepatitis B, C and alcoholic hepatitis were 162 (73.3%), 21(9.5%), 29 (13.1%); 71 (75.6%), 10 (10.6%), 8 (8.5%); and 82 (82.0%), 6 (6.0%), 2 (2.0%). The number of patients with cirrhotic is 173 (78.3%), 69 (73.4%) and 70 (70%). The median of serum AFP was 26.10 (range 0.98-25451.00) ng/mL, 9.34 (range 1.09-6740.42) ng/mL and 31.070 (range 0.713-4587.000) ng/mL. Serum total bilirubin was 12.5 (range 2.9-64.6) µmol/L, 17.4 (range 3.6-446.9) µmol/L and 13.2 (range 4.4-47.2) μmol/L. direct bilirubin was 3.9 (range 1.0-17.0) μmol/L, 4.5 (range 1.0-218.9) μmol/L and 5.50 (range 1.50-26.84) μmol/L. MELD score was 13.9 ± 4.8 (range 7.0-26.9), 13.8 ± 5.8 (range 6.0-35.5) and  $11.8 \pm 4.5$  (range 5.2-25.6). The number of patients of Child-Pugh classes A, B, and C were 205 (93.2%), 13 (5.9%), 2 (0.9%); 81 (86.2%), 12 (12.8%), 1 (1.1%) and 86 (86.0%), 13 (13.0%), 1 (1.0%) respectively. There were 32 (14.5%), 142 (64.3%), 47 (21.2%); 12 (12.8%), 68 (72.3%), 14 (14.9%) and 8 (8.0%), 71 (71.0%), 21 (21.0%) cases at histological grades I, II, and III, respectively (Table 1).

#### Conventional radiological features

In the group comparison of MVI positive and negative, the AFP and tumor size were 33.91 (range 1.4-25451.0) and 22.52 (range 0.98-18929.00) (ng/mL) (P = 0.026), 2.34 ± 0.56 and 1.92 ± 0.67 (cm) (P = 0.036) in the hospital A; 38.97 (range 1.90-6740.40) and 5.43 (range 1.10-2018.79) (ng/mL) (P = 0.01), 2.43 ± 0.57 and 2.11 ± 0.66 (cm) (P = 0.047) in the hospital B; 109.72 (range 0.80-2278.00) and 24.41 (range 0.71-4587.00) (ng/mL) (P = 0.032), 2.47 ± 0.43 and 2.21 ± 0.64 (cm) (P = 0.054) in the hospital C. In the group of MVI positive, the proportion of patients with nonsmooth tumor margin, incomplete capsule and peritumoral hypointensity was 39.7% (27/68) (P = 0.019), 40.3% (25/62) (P = 0.02) and 51.5% (17/33) (P = 0.002) in the hospital A; 52.9% (9/17) (P = 0.003), 59.5% (25/42)

(P = 0.062) and 35.7% (5/14) (P = 0.304) in the hospital B; 31.3% (10/32) (P = 0.004), 14.6% (6/41) (P = 0.759) and 63.6% (14/22) (P = 0.002) in the hospital C (Table 2).

For discriminating MVI positive, in hospital A, B and C the AUC of AFP was 0.597 [95% confidence interval (CI): 0.528-0.662], 0.683 (95%CI): 0.528-0.662] and 0.669 (95%CI: 0.568-0.760), respectively; of tumor size was 0.675 (95%CI: 0.609-0.736), 0.639 (95%CI: 0.553-0.735) and 0.576 (95%CI: 0.473-0.675), respectively; of nonsmooth tumor margin was 0.580 (95%CI: 0.512-0.646), 0.649 (95%CI: 0.544-0.745) and 0.682 (95%CI: 0.581-0.771), respectively; of incomplete capsule was 0.577 (95%CI: 0.509-0.643), 0.595 (95%CI: 0.489-0.695) and 0.521 (95%CI: 0.419-0.622), respectively; of peritumoral hypointensity on HBP was 0.582 (95%CI: 0.514-0.648), 0.551 (95%CI: 0.445-0.654) and 0.667 (95%CI: 0.565-0.758), respectively (Table 3).

#### Radiomics signatures

There were 155 and 66 patients with sHCC in the training and testing dataset, respectively. The proportion of MVI-positive patients was 27.1% and 29%, respectively. There was no significant difference in patient characteristics between the training and testing cohorts (P > 0.05). Among 1409 radiomics features in each T1WI, T2WI, DWI, AP, PVP and HBP model, 443, 483, 467, 554, 462 and 453 features were selected based on the variance threshold of over 0.80. After LASSO analysis, there were 5, 22, 33, 4, 8, and 30 features were selected for each T1WI, T2WI, DWI, AP, PVP and HBP.

#### The results of robustness analysis

70.5% (993/1409) features extracted from T1WI images had excellent consistency (ICC > 0.8), all of the 5 features that selected for modeling had excellent consistency (ICC Median was 0.969, minimum 0.877, maximum 1.000). Features of 51.9% (731/1409) extracted from T2WI images had excellent consistency (ICC > 0.8), most of the 22 features that selected for modeling had good consistency (ICC Median was 0.701, minimum 0.41, maximum 0.94). Features of 60.04% (846/1409) extracted from DWI images had excellent consistency (ICC > 0.8), most of the 33 features that selected for

modeling had excellent consistency (ICC Median was 0.869, minimum 0.41, maximum 0.98). Features of 67.8% (956/1409) extracted from AP images had excellent consistency (ICC > 0.8), the ICC of 4 features that selected for modeling was 0.902, 0.884, 0.734 and 0.891. Features of 62.1% (875/1409) extracted from PVP images had excellent consistency (ICC > 0.8), most of the 8 features that selected for modeling had excellent consistency (ICC Median was 0.844, minimum 0.500, maximum 1.000). Features of 82.5% (1163/1409) extracted from HBP images had excellent consistency (ICC > 0.8), most of the 30 features that selected for modeling had excellent consistency (ICC Median was 0.917, minimum 0.690, maximum 1.000).

### The predictive performance of the ML classifiers

The machine learning classifiers in this study were KNN, LR, MLP, RF, SVM, and DT. In general, all classifiers achieved a satisfying performance, with LR being the best machine learning method. For prediction of MVI, the T1WI, T2WI, DWI, AP, PVP and HBP radiomics model were respectively constructed and validated. In testing set, AUC was 0.776 (95%CI: 0.611-0.895), 0.813 (95%CI: 0.651-0.922), 0.971 (95%CI: 0.858-0.999), 0.788 (95%CI: 0.642-0.894), 0.790 (95%CI: 0.630-0.904) and 0.979 (95%CI: 0.911-1.000); In validation hospital B, AUC was 0.834 (95%CI: 0.742-0.904), 0.825 (95%CI: 0.732-0.896), 0.816 (95%CI: 0.678-0.876), 0.810 (95%CI: 0.715-0.884), 0.847 (95%CI: 0.758-0.913) and 0.970 (95%CI: 0.912-0.994); In validation hospital C, AUC was 0.766 (95%CI: 0.672-0.844), 0.761 (95%CI: 0.669-0.839), 0.801 (95%CI: 0.710-0.871), 0.824 (95%CI: 0.737-0.892), 0.833 (95%CI: 0.748-0.898) and 0.803 (95%CI: 0.680-0.834) (Figure 3, Table 4).

### Development and validation of MVI predicting nomogram

The C-index of radiomics and clinic combine nomogram with the model of T1WI, T2WI, DWI, AP, PVP and HBP was 0.771 (95%CI: 0.695-0.836), 0.895 (95%CI: 0.834-0.940), 0.990 (95%CI: 0.957-0.999), 0.774 (95%CI: 0.706-0.833), 0.746 (95%CI: 0.668-0.814) and 0.990 (95%CI: 0.944-0.993), in the training set; was 0.846 (95%CI: 0.594-0.883), 0.917 (95%CI: 0.640-0.915), 0.970 (95%CI: 0.843-0.997), 0.794 (95%CI: 0.615-0.876), 0.831 (95%CI: 0.650-0.650-0.876)

0.916) and 0.971 (95%CI: 0.892-0.999), in the testing set; was 0.895 (95%CI: 0.775-0.925), 0.886 (95%CI: 0.746-0.906), 0.843 (95%CI: 0.685-0.881), 0.886 (95%CI: 0.695-0.899), 0.918 (95%CI: 0.791-0.934) and 0.912 (95%CI: 0.918-0.996), in the validation\_hospital B; was 0.830 (95%CI: 0.667-0.850), 0.808 (95%CI: 0.654-0.867), 0.869 (95%CI: 0.694-0.899), 0.874 (95%CI: 0.674-0.884), 0.870 (95%CI: 0.732-0.887) and 0.808 (95%CI: 0.635-0.892), in the validation\_hospital C (Figure 4, Table 5).

The decision curve analysis showed an adequate performance for radiomics nomogram models in predicting MVI in sHCC. The proposed radiomics model to predict MVI showed a greater advantage than the "clinicoradiologic" scheme (P < 0.05). There was no significant difference in the predictive efficacy between the combination nomogram model and the single radiomics model (P > 0.05) (Figure 5).

#### **DISCUSSION**

In this multicenter study, we analyzed the clinical and imaging data of 415 patients with sHCC who underwent both DWI, Gd-EOB-DTPA-enhanced MRI and hepatectomy. We took the computer machine learning approach to construct radiomics signatures and nomogram models for preoperative prediction of MVI, then independently validated the machine learning and nomogram models. Our data showed clinical and common MRI radiological features, including AFP, tumor size, nonsmooth tumor margin, incomplete capsule and HBP peritumoral hypointensity have limited diagnostic value for MVI of sHCC. The classifier of Logistic regression (LR) was the best machine learning method, the radiomics scores of hepatobiliary phases (HBP) and DWI had the great diagnostic efficiency for predicting MVI of sHCC, the nomogram model of combined radiomics scores, APF and common MRI features which exhibited good calibration and discrimination in the training, testing and independent external validation cohorts.

Gd-EOB-DTPA with a pendant ethoxybenzyl group covalently attached to gadopentetate dimeglumine, it is the hepatocyte specific MRI contrast agent, that can be taken up by hepatocytes *via* the organic anion transporting polypeptides<sup>[30]</sup>. Gd-EOB-

DTPA with both characteristics of dual extracellular and hepatobiliary properties that provide structural and functional information for liver lesions, it can also provide the information of nonspecific gadolinium chelates during the dynamic enhancement [31,32]. Granito et al [33] reported that Gd-EOB-DTPA enhanced MRI may improve the sensitivity of the noninvasive diagnosis of small HCC nodules in patients with cirrhosis, and the double hypointensity in the portal/venous and HBP can be regarded MRI pattern, which highly suggestive hypovascular hepatocellular carcinoma. Although the study revealed that large tumor size, incomplete capsule, non-smooth tumor margin, peritumoral enhancement on AP and peritumoral hypointensity on HBP could achieve predictive AUCs of up to 0.85 for MVI of HCC[34], but for small HCC (large tumor size \leq 3 cm), the common MRI radiologic features are smooth tumor margin, complete capsule (or no capsule) and no peritumoral hypointensity in HPH. In this study, the results which came from three hospitals showed that these conventional MRI radiologic features had limited values to evaluate the MVI for sHCC.

Based on these characteristics, we established the GD-EOB-DTPA MRI Radiomics model using machine learning to construct and validate radiomics models for predicted MIV of sHCC. Machine learning demonstrated capabilities to learn and even master complex tasks, making them useful for computer-aided diagnosis and decision support systems<sup>[21]</sup>. Radiomics refers to a technique of the high-throughput extraction of quantitative imaging features or textures to decode histology and create a high-dimensional data set<sup>[35]</sup>. Although it was thought that the parameters of MRI scanner would not have obvious influence on the results of radiomics analysis after the images were standardized when the previous multicenter study<sup>[36]</sup> did not demanded the same MRI scanners and parameters. But, to minimize the possible influence of other factors, unified MRI scanner and the process of image standardization were used in our study. Furthermore, the whole-tumor volume analysis was used to decrease sampling bias. Although previous studies have verified that radiomics features of CT imaging could predict MVI status in patients with HCC preoperatively, it has a high diagnostic efficiency, and the AUC can reach about 0.85<sup>[27,37]</sup>. As well as Feng *et al* evaluated Gd-

EOB-DTPA-enhanced MRI quantitative features of peri- and intratumoural regions, providing a radiomics model for MVI prediction in HCC patients, in the validation cohort, the AUC, sensitivity, specificity was 0.83%, 90.00%, and 75.00%, respectively [38]. But none of them predicted the MVI for sHCC nor provide a clinical nomogram. In this study, we extracted radiomics signatures from images of Gd-EOB-DTPA enhanced MRI, and then built the model in T1WI, T2WI, AP, PVP, and HBP. The results illustrated that radiomics has the best modeling in HBP and DWI, when the LR and the classifier of machine learning are utilized, producing the great diagnostic efficiency for predict MVI, the results of independent external validation had confirmed that efficiency. The reason that it has the great modeling in HBP may be that the post-Gd-EOB-DTPA contrast enhancement images provides structural and functional information of HBP lesions. The LR algorithm is to establish a cost function for a classification or regression problem, and then solve the optimal model through optimization method iteratively.

Our results also demonstrated that the radiomics characteristics of DWI images can excellently predict the MVI of sHCC. DWI is an MRI technology that can reflect the motion state of water molecules in vivo, and could be used to assess tumor cellularity<sup>[39]</sup>. HCC with MVI is more likely to have higher cellularity and poor differentiation than without MVI<sup>[40]</sup>. Okamura *et al*<sup>[41]</sup> suggested apparent diffusion coefficient (ADC) value was not only a valuable predictor of poor differentiation and MVI, but also significantly related to tumor recurrence. Kim *et al*<sup>[42]</sup> illustrated that the tumour-to-liver ADC ratio was a significantly independent parameter for MVI of sHCC and the degree of lymphocyte infiltration. Our research further extracted the radiomics characteristics of the tumor which were based on the DWI images that confirmed that the quantitative characteristics of the radiomics had good performance for predicting the MVI of sHCC.

The nomogram was built in our study, which converting each regression coefficient proportionally in multivariate logistic regression to a 0- to 100-point scale. The effect of the features with the absolute value of highest  $\beta$  coefficient was assigned 100 points.

The total points of independent variables which were converted to predicted probabilities. The concordance index (C index) was used for predict the performance of nomogram, and calibration with 1000 bootstrap samples to decrease the overfit bias<sup>[43]</sup>. Our study incorporated six factors which included radiomics signatures, APF, tumor size, nonsmooth tumor margin, incomplete capsule and peritumoral hypointensity. The radiomics combined clinicoradiological factors nomogram model achieved good concordance indexes in predicting MVI in the training and validation cohorts, especially the nomogram with BPH and DWI radiomics model showed excellent predictive efficiency in the two external validation data sets, decision curve analysis further confirmed the clinical usefulness of the nomogram.

Nonetheless, there are a few of limitations in this study. Firstly, the included patient population of this study had an inevitable bias in the inter-center distribution, though the application of radiomics and clinical nomogram was ensured by the multi-center of this study, to investigate the impact factors of bias to the baseline, we analyzed the age, AFP levels, liver function and tumor size, further larger-scale researches with more balanced subjects are needed to validate our results. Secondly, given the difficulty of collecting scalable medical imaging data for small HCC, many of the patients with small HCC who received transarterial chemoembolization or ablation, we here adopted radiomics signatures and clinical nomogram to predict MVI. Given larger medical imaging datasets, deep networks would be expected to improve prediction accuracy. Thirdly, this study lacked prognostic analysis, next step we will analyze the different prognosis of sHCC patients with positive and negative MVI which been predicted by radiomics nomogram.

#### CONCLUSION

In conclusion, our study revealed that AFP and conventional Gd-EOB-DTPA enhanced MRI features have poor diagnostic accuracy for MVI in sHCC. The radiomics signatures of HBP and DWI can further improve the ability to predict MVI. Furthermore, as a noninvasive preoperative prediction method, the radiomics nomogram showed a

favorable predictive accuracy for evaluating MVI in sHCC, which may help reassess the clinical therapeutic regimen of patients with sHCC.

#### ARTICLE HIGHLIGHTS

#### Research background

Microvascular invasion (MVI) of hepatocellular carcinoma (HCC) is an independent poor prognostic factor.

#### Research motivation

It is difficult to determine MVI of small hepatocellular carcinoma (HCC) ( $\leq$  3.0 cm) by preoperative MRI conventional features.

#### Research objectives

To develop and validate radiomics scores and nomogram of gadolinium ethoxybenzyl dimeglumine (Gd-EOB-DTPA) enhanced magnetic resonance imaging (MRI) for preoperative prediction of MVI in sHCC.

#### Research methods

Radiomics models of Gd-EOB-DTPA enhanced MRI and diffusion weighted images were constructed and validated by machine learning from data sets of three hospitals. A nomogram prediction model was developed using multivariable logistic regression analysis which included the radiomics scores, radiologic features, and alpha-fetoprotein (AFP) level.

#### Research results

AFP and MRI conventional features had poor diagnostic value for MVI of small HCC. The nomogram model (combined radiomics and clinic features) exhibited good calibration and discrimination in the testing and two external validation cohorts (in the two external validation cohorts, C-index was 0.912 and 0.808, respectively).

#### Research conclusions

As a noninvasive preoperative prediction method, the MRI radiomics nomogram shows favorable predictive accuracy for evaluate MVI in sHCC.

#### Research perspectives

This clinical prediction model may help in the selection of treatment options for small HCC.

#### **ACKNOWLEDGEMENTS**

The authors would like to thank Yingying Ezell for the language recheck and editing, Fuling Huang for his technical support, and Huiting Zhang (Siemens Healthineers, Wuhan, Hubei, China) for her constructive suggestions during the MRI scanning.

#### **Figure Legends**

Figure 1 Flow diagram of the study cohort. A total of 415 participants were included in this multi-center study.

Figure 2 Flow diagram for the radiomics of machine learning. A: Construct radiomics models, the volume of interest was delineated by experienced radiologists and three-dimensional images were formed, extracting quantitative features by software; B: Pathologic examination, firstly obtaining specimens of small hepatocellular carcinoma tissue, and then taking pathologic diagnosis for microvascular invasion; C: Data cleaning and dimensions reduction; D: Establishing the model for predicting microvascular invasion by machine learning. LR: Logistic regression; KNN: K-Nearest neighbor; SVM: Support vector machin; RF: Random forest.

Figure 3 Receiver operating characteristic curve of different radiomics models for diagnosis microvascular invasion in small hepatocellular carcinoma (testing set). A:

T1 weighted imaging [area under curve (AUC) was 0.776; 95% confidence interval (CI): 0.611-0.895]; B: T2 weighted imaging [AUC, 0.813; 95% confidence interval (CI): 0.651-0.922]; C: Diffusion weighted imaging (AUC, 0.971; 95%CI: 0.858-0.999); D: Arterial phase (AUC, 0.788; 95%CI: 0.642-0.894); E: Portal vein phase (AUC, 0.790; 95%CI: 0.630-0.904); F: Hepatobiliary phase (AUC, 0.990; 95%CI: 0.911-1.000). T1W1: T1 weighted imaging; T2W2: T2 weighted imaging; AUC: Area under curve; DWI: Diffusion weighted imaging; AP: Arterial phase; PVP: Portal vein phase; HBP: Hepatobiliary phase.

Figure 4 Nomogram of diffusion weighted imaging radiomics model to predict microvascular invasion in patients with small hepatocellular carcinoma. A: The nomogram was developed with radiomics signature and clinicoradiological factors. A vertical line was drawn according to the value of radiomics scores to determine the corresponding value of points. Similarly, the points of tumor markers were determined. The total points were the sum of the two points above. Finally, a vertical line was made according to the value of the total points to determine the probability of microvascular invasion (MVI); B: Validity of the predictive performance of the nomogram in estimating the risk of MVI presence in the training cohort; C: Validity of the predictive performance of the nomogram in estimating the risk of MVI presence in the validation cohort. AFP: Alpha-fetoprotein; DWI: Diffusion weighted imaging; Rad\_score: Radiomics signatures score.

Figure 5 Decision curve analysis. A and B: Decision curve analysis of the prediction model for training (A) and testing (B) cohort. Y-axis represents the net benefit, which is calculated by gaining true positives and deleting false positives. The X-axis is the probability threshold. The curve of the radiomics and combined nomogram over the clinical features that integrated AFP and radiological signatures showed the greatest benefit. AFP: Alpha-fetoprotein; Rad\_score: Radiomics signatures score.

Table 1 Demographics, alpha fetal protein, bilirubin, tumor characteristics, and microvascular infiltration of the patients with small hepatocellular carcinoma in data sets of three hospitals

$ \begin{array}{llllllllllllllllllllllllllllllllllll$
$ \begin{array}{cccccccccccccccccccccccccccccccccccc$
Male/female       (14.5%)       84 (89.4%)/10 (10.6%)       (15.0%)         Causes of liver disease       (15.0%)       82 (82.0%)         Hepatitis B       162 (73.3%)       71 (75.6%)       82 (82.0%)         Hepatitis C       21 (9.5%)       10 (10.6%)       6 (6.0%)         Alcoholic hepatitis       29 (13.1%)       8 (8.5%)       2 (2.0%)         Others       9 (4.1%)       5 (5.3%)       10 (10.0%)         Cirrhosis         Present       173 (78.3%)       69 (73.4%)       70 (70%)
Causes of liver disease  Hepatitis B 162 (73.3%) 71 (75.6%) 82 (82.0%)  Hepatitis C 21 (9.5%) 10 (10.6%) 6 (6.0%)  Alcoholic
$\begin{array}{llllllllllllllllllllllllllllllllllll$
Hepatitis C       21 (9.5%)       10 (10.6%)       6 (6.0%)         Alcoholic hepatitis       29 (13.1%)       8 (8.5%)       2 (2.0%)         Others       9 (4.1%)       5 (5.3%)       10 (10.0%)         Cirrhosis         Present       173 (78.3%)       69 (73.4%)       70 (70%)
Alcoholic hepatitis  Others 9 (4.1%) 5 (5.3%) 2 (2.0%)  Cirrhosis  Present 173 (78.3%) 69 (73.4%) 70 (70%)
hepatitis       29 (13.1%)       8 (8.5%)       2 (2.0%)         Others       9 (4.1%)       5 (5.3%)       10 (10.0%)         Cirrhosis         Present       173 (78.3%)       69 (73.4%)       70 (70%)
hepatitis Others 9 (4.1%) 5 (5.3%) 10 (10.0%) Cirrhosis Present 173 (78.3%) 69 (73.4%) 70 (70%)
Cirrhosis  Present 173 (78.3%) 69 (73.4%) 70 (70%)
Present 173 (78.3%) 69 (73.4%) 70 (70%)
Absent 48 (21.7%) 25 (26.6%) 30 (30%)
== (======)
Median: 26.10 (range Median: 9.34 (range
AFP (ng/mL) (range 0.713-0.98-25451.00) 1.09-6740.42)
4587.000)
Median: 12.5 (range Median: 17.4 (range Median: 13.2 (range TBiL (μmol/L)
2.9-64.6) 3.6-446.9) 4.4-47.2)
DBiL (μmol/L)  Median: 3.9 (range Median: 4.5 (range 1.0- Median: 5.50 (range
1.0-17.0) 218.9) 1.50-26.84)
mean $\pm$ SD: 13.9 $\pm$ 4.8 mean $\pm$ SD: 13.8 $\pm$ 5.8 mean $\pm$ SD: 11.8 $\pm$ MELD scores
(range 7.0-26.9) (range 6.0-35.5) 4.5 (range 5.2-25.6)
Child-Pugh classes
A 205 (93.2%) 81 (86.2%) 86 (86.0%)
B 13 (5.9%) 12 (12.8%) 13 (13.0%)

C 11	2 (0.9%)	1 (1.1%)	1 (1.0%)
Edmondson-stein	er grade		
Grade I	32 (14.5%)	12 (12.8%)	8 (8.0%)
Grade II	142 (64.3%)	68 (72.3%)	71 (71.0%)
Grade III	47 (21.2%)	14 (14.9%)	21 (21.0%)
Tumor size (cm)	mean ± SD: 2.04 ±	mean $\pm$ SD: 2.17 $\pm$ 0.42	mean ± SD: 2.20 ±
Tullior size (cili)	0.67 (range 0.60-3.00)	(range 0.80-3.00)	0.41 (range 0.90-3.00)
MVI			
Positive	64 (28.9%)	22 (23.4%)	16 (16.0%)
Negative	157 (71.1%)	72 (76.6%)	84 (84.0%)

TBiL: Total bilirubin; DBiL: Direct bilirubin; MELD: Model for end-stage liver disease;

 $AFP: Alpha-fetoprotein; MVI: Microvascular\ infiltration.$ 

Table 2 Age, gender, alpha-fetoprotein and radiologic features of patients with small hepatocellular carcinoma and relationship with microvascular infiltration

	Hospital A $(n = 221)$	1 = 221)		Hospital B $(n = 94)$	(n = 94)		Hospital C $(n = 100)$	= 100)	
	38		Ь			Ь			Р
	Positive	Negative	value	Positive	Negative	value	Positive	Negative	value
Age (yr)	$50.9 \pm 10.7$	$51.3 \pm 10.9$	0.840	$51.7 \pm 12.3$	$53.1 \pm 10.1$	0.597	$53.5 \pm 9.1$	$53.7 \pm 11.0$	0.958
Gender			0.593			0.443			0.259
Female	8	24		1	6		1	14	
Male	56	133		21	63		15	70	
	33.91 (range	22.52		38.97	5.43 (range		109.72	24.41	
AFP (ng/mL) 1.40-	1.40-	(range 1- 0.026	0.026	(range 1 90-	1.10-	0.010	(range 0.80-	(1411ge 0 71-	0.032
	25451.00)	18929)		6740.40)	2018.79)		2278.00)	4587.00)	
Size (cm)	$2.34 \pm 0.56$	$1.92 \pm 0.67  0.036$	0.036	$2.43 \pm 0.57$	$2.11\pm0.66$	0.047	$2.47 \pm 0.43$	$2.21 \pm 0.64$	0.054
Nonsmooth									
tumor			0.019			0.003			0.004
margin									
Absent	37	116		13	64		9	62	
Present	27	41		6	8		10	22	
Capsule			0.020			0.062			0.756

Absent	39	120	21	55	10	49
Present	25	37	25	17	9	35
Peritumoral		000		706.0		0000
hypointensity		0.002		£00.0		0.00
Absent	47	141	17	63	70	8
Present	17	16	5	6	14	8

Size: Large tumor size; AFP: Alpha-fetoprotein; MVI: Microvascular infiltration.

Table 3 Diagnostic performance of alpha-fetoprotein and radiologic features for assessing microvascular infiltration of small hepatocellular carcinoma by receiver operating characteristic curve analysis

	AFP Tumor size tumor margin			Incomplete	Peritumoral
			margin	capsule	hypointensity
Hospital A					
AUC	0.597	0.675	0.580	0.577	0.582
95% CI	0.528-0.662	0.609-0.736	0.512-0.646	0.509-0.643	0.514-0.648
P value	0.024	< 0.001	0.024	0.027	0.007
Sensitivity	34.92	70.31	42.19	39.06	26.56
Specificity	81.82	61.15	73.89	76.43	89.81
Hospital B					
AUC	0.683	0.639	0.649	0.595	0.551
95% CI	0.577-0.777	0.553-0.735	0.544-0.745	0.489-0.695	0.445-0.654
P value	0.006	0.035	0.008	0.005	0.304
Sensitivity	63.64	81.82	71.43	95.45	22.73
Specificity	72.06	44.44	88.89	23.61	87.50
Hospital C					
AUC	0.669	0.576	0.682	0.521	0.667
95% CI	0.568-0.760	0.473-0.675	0.581-0.771	0.419-0.622	0.565-0.758
P value	0.016	0.213	0.007	0.759	0.014
Sensitivity	87.50	68.75	62.50	62.50	50.00
Specificity	52.38	54.76	73.81	41.67	83.33

DeLong test for comparison of receiver operating characteristic curve. AFP: Alphafetoprotein; AUC: Area under the curve; 95%CI: 95% confidence interval.

Table 4 Receiver operator characteristic curve analysis of radiomics scores with different sequences of magnetic resonance imaging for predict microvascular infiltration of small hepatocellular carcinoma

	T1WI	T2WI	DWI	AP	PVP	HBP
Training set						
AUC	0.740	0.878	0.991	0.763	0.739	0.976
95%CI	0.661-	0.814-	0.958-	0.695-	0.661-	0.940-
	0.808	0.926	0.999	0.823	0.807	0.991
P value	< 0.001	< 0.001	< 0.001	< 0.001	< 0.001	< 0.001
Sensitivity	77.08	82.98	95.74	71.43	56.25	89.83
Specificity	68.00	82.00	96.04	79.37	78.22	99.27
Testing set						
AUC	0.776	0.813	0.971	0.788	0.790	0.979
95%CI	0.611-	0.651-	0.858-	0.642-	0.630-	0.911-
	0.895	0.922	0.999	0.894	0.904	1.000
P value	0.0004	< 0.001	< 0.001	0.0014	0.0001	< 0.001
Sensitivity	91.67	58.33	100.00	64.29	84.62	100.00
Specificity	57.69	92.00	84.62	93.75	73.08	91.43
Validation_Hospital B						
AUC	0.834	0.825	0.816	0.810	0.847	0.970
95%CI	0.742-	0.732-	0.678-	0.715-	0.758-	0.912-
	0.904	0.896	0.876	0.884	0.913	0.994
P value	< 0.001	< 0.001	0.0002	< 0.001	< 0.001	< 0.001
Sensitivity	63.64	95.45	71.43	57.14	54.55	95.45
Specificity	94.29	57.75	88.89	88.89	98.61	98.57
Validation_Hospital C						
AUC	0.766	0.761	0.801	0.824	0.833	0.803
95%CI	0.672-	0.669-	0.710-	0.737-	0.748-	0.680-
	0.844	0.839	0.871	0.892	0.898	0.834

P value	0.0001	0.0003	< 0.001	< 0.001	< 0.001	0.007
Sensitivity	80.00	60.00	90.00	86.67	85.71	83.33
Specificity	70.45	89.01	68.89	68.54	72.83	77.67

T1WI: T1 weighted imaging; T2WI: T2 weighted imaging; DWI: Diffusion weighted imaging; AP: Arterial phase; PVP: Portal vein phase; HBP: Hepatobiliary phase; AUC: Area under the curve; 95%CI: 95% confidence interval.

Table 5 Predictive performance of the nomogram prediction model for estimating the risk of microvascular infiltration presence in patients with small hepatocellular carcinoma

	<b></b>		Validation_Hospital	Validation_Hospital
	Training set	Testing set	В	C
T1WI				
C-index	0.771	0.846	0.895	0.830
95%CI	0.695-0.836	0.594-0.883	0.775-0.925	0.667-0.850
P value	< 0.001	0.0014	< 0.001	0.0001
T2WI				
C-index	0.895	0.917	0.886	0.808
95%CI	0.834-0.940	0.640-0.915	0.746-0.906	0.654-0.867
P value	< 0.001	0.0001	< 0.001	0.0015
DWI				
C-index	0.990	0.970	0.843	0.869
95%CI	0.957-0.999	0.843-0.997	0.685-0.881	0.694-0.899
P value	< 0.001	< 0.001	0.0001	< 0.001
AP				
C-index	0.774	0.794	0.886	0.874
95%CI	0.706-0.833	0.615-0.876	0.695-0.899	0.674-0.884
P value	< 0.001	0.0025	< 0.001	< 0.001
PVP				
C-index	0.746	0.831	0.918	0.870
95%CI	0.668-0.814	0.650-0.916	0.791-0.934	0.732-0.887
P value	< 0.001	< 0.001	< 0.001	< 0.001
HBP				
C-index	0.990	0.971	0.912	0.808
95%CI 53	0.944-0.993	0.892-0.999	0.918-0.996	0.635-0.892
P value	< 0.001	< 0.001	< 0.001	0.0081

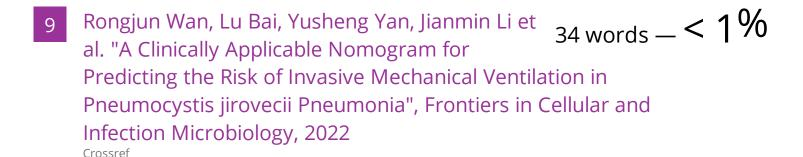
T1WI: T1 weighted imaging; T2WI: T2 weighted imaging; DWI: Diffusion weighted imaging; AP: Arterial phase; PVP: Portal vein phase; HBP: Hepatobiliary phase; 95%CI, 95% confidence interval; C-index: Concordance index.

## 74110\_Auto\_Edited-check.docx

ORIG	ΙΝΙΛΙ	ITV	DED	$\cap$ DT
OINIO		_	INLE	OIL

27% SIMILARITY INDEX

SIMILA	RITY INDEX	
PRIMA	RY SOURCES	
1	link.springer.com Internet	315 words — <b>4%</b>
2	"ECR 2019: Book of Abstracts", Insights into Imaging, 2019 Crossref	296 words — <b>4%</b>
3	www.ncbi.nlm.nih.gov Internet	197 words — <b>3</b> %
4	www.science.gov Internet	109 words — <b>1%</b>
5	Yidi Chen, Xiali Qin, Liling Long, Ling Zhang, Zhongkui Huang, Zijian Jiang, Chenhui Li. "Diagnostic Value of Gd - EOB - DTPA - Enhanced M Expression of Ki67 and Microvascular Density in He Carcinoma", Journal of Magnetic Resonance Imagin	patocellular
6	www.frontiersin.org Internet	82 words — <b>1%</b>
7	jamanetwork.com Internet	81 words — <b>1</b> %
8	pubmed.ncbi.nlm.nih.gov	59 words — <b>1%</b>



10 www.semanticscholar.org

- $_{33 \text{ words}}$  -<1%
- Likun Cao, Jie Chen, Ting Duan, Min Wang, Hanyu Jiang, Yi Wei, Chunchao Xia, Xiaoyue Zhou, Xu Yan, Bin Song. "Diffusion kurtosis imaging (DKI) of hepatocellular carcinoma: correlation with microvascular invasion and histologic grade", Quantitative Imaging in Medicine and Surgery, 2019

  Crossref
- 12 Xu Fang, Xiao Li, Yun Bian, Xiang Ji, Jianping Lu. "Radiomics nomogram for the prediction of 2019 novel coronavirus pneumonia caused by SARS-CoV-2", European Radiology, 2020  $_{\text{Crossref}}$
- cancerimagingjournal.biomedcentral.com
- 31 words < 1%
- Victoria Chernyak, An Tang, Richard K. G. Do, Aya Kamaya et al. "Liver imaging: it is time to adopt standardized terminology", European Radiology, 2022

  Crossref
- 15 wjgnet.com

- 25 words < 1%
- bmcmedimaging.biomedcentral.com

  24 words < 1 %



- Jun Shu, Didi Wen, Yibin Xi, Yuwei Xia, Zhengting Cai, Wanni Xu, Xiaoli Meng, Bao Liu, Hong Yin. "Clear cell renal cell carcinoma: Machine learning-based computed tomography radiomics analysis for the prediction of WHO/ISUP grade", European Journal of Radiology, 2019 Crossref
- Meng Yan, Xiao Zhang, Bin Zhang, Zhijun Geng et al. "A Deep Learning Nomogram for the Prediction of Early Recurrence in Hepatocellular Carcinoma After Curative Surgery", Research Square Platform LLC, 2021

  Crossref Posted Content
- www.annualreviews.org 23 words < 1 %
- www.dirjournal.org 23 words < 1 %
- Jiang Huang, Yidi Chen, Yuying Zhang, Jinhuan Xie et al. "Comparison of clinical-computed tomography model with 2D and 3D radiomics models to predict occult peritoneal metastases in advanced gastric cancer", Abdominal Radiology, 2021  $_{Crossref}$

Crossref

Ying Zhao, Jingjun Wu, Qinhe Zhang, Zhengyu Hua  $_{21~words} - < 1\%$  et al. "Radiomics Analysis Based on Multiparametric for Predicting Early Recurrence in Hepatocellular Carcinoma After Partial Hepatectomy ", Journal of Magnetic Resonance Imaging, 2020  $_{Crossref}$ 

- www.unboundmedicine.com

  18 words < 1 %
- Pengyi Yu, Xinxin Wu, Jingjing Li, Ning Mao et al.
  "Extrathyroidal Extension Prediction of Papillary
  Thyroid Cancer With Computed Tomography Based Radiomics
  Nomogram: A Multicenter Study", Frontiers in Endocrinology,
  2022
  Crossref
- Wenyue Duan, Bingdi Xiong, Ting Tian, Xinyun Zou, Zhennan He, Ling Zhang. "Radiomics in Nasopharyngeal Carcinoma", Clinical Medicine Insights:

  Oncology, 2022

  Crossref
- Www.dovepress.com

- Xin Zhao, Xueyuan Wang, Bohao Zhang, Xianglong Liu, Desheng Xuan, Yuwei Xia, Xiaoan Zhang. "Classifying early stages of cervical cancer with MRI-based radiomics", Magnetic Resonance Imaging, 2022

  Crossref
- Ji Young Choi, Jiyeon Ha, Sang Hyun Choi, Hyo Jeong Kang, So Yeon Kim, Kyoung Won Kim. "Comparison of gadoxetate disodium-enhanced MRI sequences for measuring hepatic observation size and its implication of LI-RADS classification", Abdominal Radiology, 2022
- Kun Lv, Xin Cao, Peng Du, Jun-Yan Fu, Dao-Ying Geng, Jun Zhang. "Radiomics for the detection of microvascular invasion in hepatocellular carcinoma", World Journal of Gastroenterology, 2022
- Sunyoung Lee, Tae Wook Kang, Kyoung Doo Song, Min Woo Lee et al. "Effect of Microvascular Invasion Risk on Early Recurrence of Hepatocellular Carcinoma After Surgery and Radiofrequency Ablation", Annals of Surgery, 2021 Crossref
- www.hindawi.com
  Internet

  15 words < 1 %
- bsdwebstorage.blob.core.windows.net

  14 words < 1 %
- Ji Yoon Moon, Ji Hye Min, Young Kon Kim, Donglk Cha et al. "Prognosis after Curative Resection of Single Hepatocellular Carcinoma with A Focus on LI-RADS

## Targetoid Appearance on Preoperative Gadoxetic Acid-Enhanced MRI", Korean Journal of Radiology, 2021

Crossref

- Jin Li, Yang Zhou, Xinxin Wang, Meijuan Zhou, Xi Chen, Kuan Luan. "An MRI-based multi-objective radiomics model predicts lymph node status in patients with rectal cancer", Abdominal Radiology, 2020 Crossref
- www.jmir.org 13 words < 1 %
- "ESMRMB 2008 Congress, Valencia, Spain, 2–4
  October: EPOSGäó Posters / Info-RESO",
  Magnetic Resonance Materials in Physics, Biology and
  Medicine, 2008
  Crossref
- "Posters", Hepatology, 2020
  Crossref 12 words < 1%
- Okamura, Shusuke, Shuji Sumie, Tatsuyuki Tonan, 12 words < 1 % Masahito Nakano, Manabu Satani, Shigeo Shimose, Tomotake Shirono, Hideki Iwamoto, Hajime Aino, Takashi Niizeki, Nobuyoshi Tajiri, Ryoko Kuromatsu, Koji Okuda, Osamu Nakashima, and Takuji Torimura. "Diffusion-weighted magnetic resonance imaging predicts malignant potential in small hepatocellular carcinoma", Digestive and Liver Disease, 2016.
- Zhenpeng Peng, Chang Li, Tao Chan, Huasong Cai, Yanji Luo, Zhi Dong, Zi-Ping Li, Shi-Ting Feng. 12 words <1% "Quantitative evaluation of Gd-EOB-DTPA uptake in focal liver lesions by using T1 mapping: differences between

hepatocellular carcinoma, hepatic focal nodular hyperplasia and cavernous hemangioma", Oncotarget, 2017

Crossref

- "ECR 2013 Book of Abstracts B Scientific Sessions", Insights into Imaging, 2013.

  Crossref 11 words -<1%
- Yu Liu, Dan Wang, Hong Lei Guo, Lu Hao et al. 11 words <1% "Risk factors and nomogram for diabetes mellitus in idiopathic chronic pancreatitis", Journal of Gastroenterology and Hepatology, 2019
- Granito, A., M. Galassi, F. Piscaglia, L. Romanini, V. 10 words < 1 % Lucidi, M. Renzulli, A. Borghi, L. Grazioli, R. Golfieri, and L. Bolondi. "Impact of gadoxetic acid (Gd-EOB-DTPA)-enhanced magnetic resonance on the non-invasive diagnosis of small hepatocellular carcinoma: a prospective study", Alimentary Pharmacology & Therapeutics, 2013.
- onlinelibrary.wiley.com

  10 words < 1 %
- "WORLD TRANSPLANT CONGRESS 2006 POSTER ABSTRACTS", American Journal of Transplantation, 8/2006 Crossref
- Sunyoung Lee, Kyoung Won Kim, Woo Kyoung Jeong, Myeong-Jin Kim, Gi Hong Choi, Jin Sub Choi, Gi-Won Song, Sung-Gyu Lee. "Gadoxetic acid-enhanced MRI as a predictor of recurrence of HCC after liver transplantation", European Radiology, 2019 Crossref

53 www.longdom.org

Crossref

9 words -<1%

Rui-zhe Zheng, Zhi-jie Zhao, Xi-tao Yang, Shao-wei Jiang et al. "Initial CT-based radiomics nomogram for predicting in-hospital mortality in patients with traumatic brain injury: a multicenter development and validation study", Neurological Sciences, 2022

Ryotaro Ikeguchi, Yuko Shimizu, Satoru Shimizu, Kazuo Kitagawa. "CSF and clinical data are useful in differentiating CNS inflammatory demyelinating disease from CNS lymphoma", Multiple Sclerosis Journal, 2017

Siye Liu, Xiaoping Yu, Songhua Yang, Pingsheng
Hu, Yingbin Hu, Xiaoyan Chen, Yilin Li, Zhe Zhang,
Cheng Li, Qiang Lu. "Machine Learning-Based Radiomics
Nomogram for Detecting Extramural Venous Invasion in Rectal
Cancer", Frontiers in Oncology, 2021

Crossref

"Abstract", Medical Physics, 2021 7 words - < 1%

- "ECR 2014, Part B", Insights into Imaging, 2014. 7 words < 1%
- Yidi Chen, Basen Li, Zijian Jiang, Hui Li, Yiwu Dang, Cheng Tang, Yuwei Xia, Huiting Zhang, Bin Song, Liling Long. "Multi-parameter diffusion and perfusion magnetic resonance imaging and radiomics nomogram for preoperative

# evaluation of aquaporin-1 expression in rectal cancer", Abdominal Radiology, 2022

Crossref

Chenjun Huang, Meng Fang, Xiao Xiao, Hong Wang, 6 words — < 1 % Zhiyuan Gao, Jun Ji, Lijuan Liu, Erli Gu, Ya Li, Mengmeng Wang, Chunfang Gao. "Validation of the GALAD model for early diagnosis and monitoring of hepatocellular carcinoma in Chinese multicenter study", Liver International, 2021

Crossref

EXCLUDE QUOTES OFF EXCLUDE SOURCES OFF
EXCLUDE BIBLIOGRAPHY OFF EXCLUDE MATCHES OFF